Formation and Growth of Clusters of Sulfur Dioxide

Jarle Harnes, Mahmoud Abu-Samha,* Mathias Winkler, and Knut J. Børve
Department of Chemistry, University of Bergen, Bergen, Norway

Formation and growth of neutral SO_2 clusters is investigated in an adiabatic-expansion setup by means of sulfur 2p (S2p) photoelectron spectroscopy and theoretical modeling. The shift in S2p ionization energy between the cluster and a single molecule, i.e., IE(cluster)-IE(monomer), is recorded and used to monitor the mean cluster size over a wide range of expansion conditions. The produced clusters were shown to fall into two different size regimes. Comparison between theoretical simulations and experimental observations suggests that while the smallest clusters belong to the ultrafine particle mode and have a liquid-like structure, the larger clusters belong to the accumulation mode of fine particles and possibly have a frozen cluster core. The transition between the two size/structure regimes occurs over a narrow interval in expansion conditions and may possibly reflect a change in growth mechanism from monomer addition to growth by cluster-cluster collisions.

1. INTRODUCTION

Clusters are aggregates of atoms and molecules, containing from a few to millions of building units (Johnston 2002) and ranging in size from less than a nanometer to the lower-micron scale (Finlayson-Pitts 2009). In this very concrete sense, clusters bridge the gap between atoms and molecules and the condensed phases. Clusters often possess properties different from those of their constituent building blocks and also different from the corresponding condensed phases. An example is the melting point, which, for many systems, is found to increase with cluster size (Shvartsburg and Jarrold 2000; Nanda et al.

2002; Mei and Lu 2007). Other examples are the valence and core-level ionization potentials that have been found to vary systematically with cluster size (Björneholm et al. 1996; Harnes et al. 2011).

By following the evolution of a physical or chemical property with cluster size, one may learn how the corresponding macroscopic property derives from that of the atomic or molecular building unit. Conversely, to some degree, by controlling the size and composition of the cluster one can control the size-dependent properties. The possibility to tune properties by size is one of the features that make clusters interesting to nanoscience, the other being their extreme surface-to-bulk ratio (Haberland 1994-1995a; Johnston 2002).

For *in situ* studies, a much-used approach to produce clusters is to expand a gas adiabatically through a nozzle into vacuum. Under favorable stagnation conditions, the expanding gas becomes highly supersaturated and clusters may form. Based on assumptions of cluster growth through sequential addition of monomers and cluster break-up by uniparticle spontaneous decay (Pauly 2000, p. 144), Hagena et al. introduced the concept of corresponding jets, to be characterized by the dimensionless condensation parameter, Γ^* (Hagena 1969; Hagena and Obert 1972; Hagena 1974a, b, 1981, 1987, 1992). According to this model, expansion conditions that share the same Γ^* value give rise to clusters with the same terminal mean size, $\langle N \rangle$.

Recently, we explored the use of inner-shell X-ray photoelectron spectroscopy (XPS) to monitor the mean size of CO_2 clusters (Harnes et al. 2011). For CO_2, the cluster-to-monomer shift in C1s ionization energy, ΔIE, was found to grow smoothly with both Γ^* and the terminal mean cluster size, $\langle N \rangle$. The empirical ΔIE-$\langle N \rangle$ relationship was found in good agreement with independent theoretical calculations on model clusters of size $N = \langle N \rangle$. It may be noted that core-level photoelectron spectroscopy is not affected by cluster breakup following ionization, due to the short lifetime of the core hole. Another promising approach to circumvent the fragmentation problem when determining cluster size is described in Yoder et al. (2011).

The motivation for the present contribution is the need for fundamental insight to the process of forming molecular

451

clusters and in particular the transition in size from the ultra-fine particle mode to the Aitken nuclei or accumulation modes of fine particles (Finlayson-Pitts and Pitts, Jr. 2000). SO_2 is a key compound from the aspect of atmospheric particulate matter (Kulmala et al. 2000; Berndt et al. 2005; Ota and Richmond 2011), and mixed water/SO_2 clusters are also important in the formation of acid rain (Dong et al. 2006; Ota and

Richmond 2011). More to the point of this study, sulfur dioxide is a convenient compound for exploring cluster formation over a wide range of conditions, partly because the high boiling point (263.13 K) (Yaws 1999) facilitates access to the strongly clustering regime without use of a carrier gas. Hitherto, neutral free SO_2 clusters have been studied either in the oligomeric regime (Dong et al. 2006) or, motivated by the importance in planetary atmospheres, in the large-cluster regime (Fleyfel et al. 1990; Signorell and Jetzki 2008). In contrast, here we explore how the mean size $\langle N \rangle$ of SO_2 clusters produced in adiabatic expansion evolves over a wide range of experimental conditions. The large cross section of the sulfur 2p photoemission process makes XPS well suited for monitoring the mean cluster size. Different from the spatial or temporal resolution offered in some studies (Paci et al. 2004; Laksmono et al. 2011; Pathak et al. 2013; Ezell et al. 2014), the cluster beam is probed at a fixed distance about 10 cm downstream from the nozzle neck, i.e., at a mature particle population.

2. EXPERIMENTS

In 2009, we recorded S2p photoelectron spectra of neutral free SO_2 clusters at five different expansion conditions. The series was greatly expanded one year later. Pure SO_2 gas was expanded into vacuum through a small conical nozzle with an opening diameter of 150 μm, a total opening angle of 20°, and a length of the diverging section of 2 cm (Tchaplyguine et al. 2003). The expansion leads to a lowering of the rotational and translational temperature of the gas (Pauly 2000, p. 129), which, together with the initially large number of two- and three-body collisions, leads to nucleation followed by cluster growth. The flow of molecules and clusters is led through a 300 μm skimmer, which extracts the central cluster-rich part of the flow and produces a beam of clusters and uncondensed molecules, subsequently to be probed by S2p photoelectron spectroscopy.

In 2009, the temperature on the nozzle, T_n, was measured to be 301 ± 1 K, while the pressure in the stagnation chamber, P_0, was varied between 510 and 1970 mbar. In the 2010 experiments, T_n was kept around 290 K while P_0 was varied from 200 mbar to 2420 mbar. In order to compensate for possible time-dependent variations in the experimental conditions, the 2010 spectra were recorded at alternating low and high P_0 values. In the online supplemental information (SI), it is shown that with our setup and assuming that the stagnation

temperature is given by the temperature of the nozzle, the Γ^* condensation parameter relates to the experimental conditions by Equation (1).

$$\Gamma^*_{SO_2} = 1.08 \times 10^9 \left(\frac{P_0}{mbar}\right)\left(\frac{T_0}{K}\right)^{-3.4} \quad [1]$$

Figure 1 shows the experimental settings superimposed on a contour plot of the Γ^* condensation parameter.

The photoelectron spectra were recorded at the I411 undulator beamline (Bässler et al. 1999, 2001) of the MAX II storage ring located at MAX-lab in Lund, Sweden, using a photon energy of 200 eV. The beamline is equipped with a modified SX-700 monochromator and the photoelectrons are detected using a Scienta R4000 hemispherical electron analyzer. We used a monochromator slit opening of 25 μm and a pass energy E_{pass} of 50 eV for the analyzer. The instrumental broadening based on these experimental settings is approximately Gaussian and with a full-width-at-half-maximum (fwhm) around 90 meV. The binding energy is calibrated to the vertical ionization energies for the $S2p_{3/2}$ and $S2p_{1/2}$ levels in gaseous SO_2, which are reported as 174.78 ± 0.03 eV and 175.99 ± 0.03 eV, respectively (Coville and Thomas 1995).

2.1. Fitting Models

The photoelectron spectra contain signals from both uncondensed molecules, i.e., monomers, and clusters. In order to extract the cluster component, each spectrum was fitted in terms of a monomer spectrum that was recorded under similar conditions, and a model cluster spectrum. The latter was prepared from a monomer spectrum by convolution with a Gaussian distribution to account for the distribution of ionization energies within a cluster and excitations of intermolecular
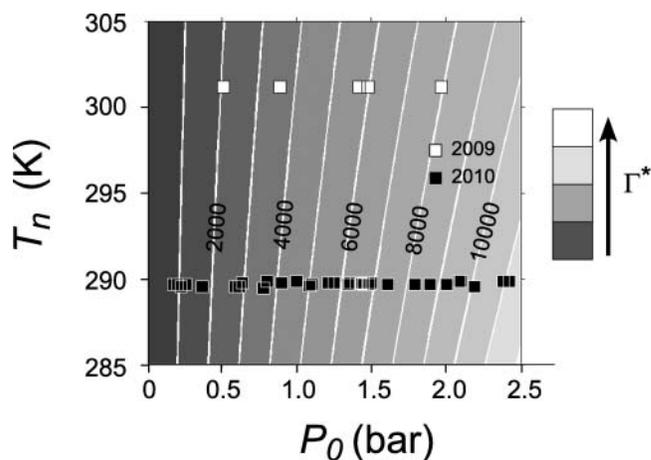

FIG. 1. Contour plot of the condensation parameter (Γ^*) (Hagena and Obert 1972; Hagena 1981, 1987) as a function of the nozzle temperature, T_n, and stagnation pressure, P_0. Experimental conditions are shown as open or filled squares, representing experiments conducted in 2009 and 2010, respectively.

vibrational modes following ionization (Bergersen et al. 2006b), and also additional broadening due to the distribution of cluster sizes in the beam. A total of five free parameters were used in the fitting procedure: peak height, position and Gaussian width of the cluster component, the peak height of the monomer component, and a constant background.

3. COMPUTATIONS

Molecular dynamics simulations were conducted with canonical-ensemble conditions to obtain realistic distributions of SO_2 cluster geometries. Using the dynamic program in the Tinker suite of programs version 5.1 (Ponder and Richards 1987), cluster geometries with 13, 55, 147, 309, and 561 molecules were propagated at three different temperatures (100 K, 125 K, 150 K). For this purpose, the AMOEBA (Ponder et al. 2010) force field was parametrized for both neutral and S2p-ionized SO_2 as detailed in the SI, which also contains results from validation tests for both oligomer structures, crystal density, and chemical shifts in S2p energies. AMOEBA contains an electrostatic distributed-multipole model, with charge, dipole, and quadrupole at each atomic site. All simulations were carried out in the rigid-body approximation with 5 fs timesteps. Initial structures were prepared by building cuboctahedrons with the molecules randomly oriented in space and placed at an fcc grid with an inter-gridpoint distance of 5 Å. First, the simulations ran for 1 ns at 150 K. Next, the temperature was lowered to 125 K at a rate of 1 K/ps using the anneal option in Tinker. At this temperature, the simulation ran for 1 ns before a second annealing step followed. Finally, the simulations ran for 1 ns at 100 K.

3.1. Attenuation Model

For quantitative use of photoelectron spectroscopy on condensed systems, attenuation of the photoelectron signal due to interaction with matter needs to be taken into account. The attenuation of the photoelectron signal is usually modeled by an exponential *Ansatz* as $I/I_o = \exp(-d/\lambda)$ (Amar et al. 2005; Bergersen et al. 2006a; Harnes et al. 2011), where d is the distance traveled by the photoelectron through matter and λ denotes the signal attenuation length. An upper bound to λ may be obtained as $\lambda = 1/\sigma_i n$, where σ_i is the cross section for inelastic collisions between an electron and SO_2 and n is the number density at the expected structure and temperature. While the inelastic scattering cross section is obtained as the difference between the total and the elastic cross sections (Bhardwaj and Michael 1999), the number density is taken to be that of the solid at 143 K (0.030 mol cm^{-3}) (Post et al. 1952). The effect of elastic scattering is to increase the distance that the electron travels before escaping from the cluster.

If elastic scattering were neglected, one would arrive at an upper bound of 12.0 Å for λ. We have modeled the effect of elastic scattering by Monte Carlo simulations of the propagation of electrons through an $N = 561$ cluster following the approach outlined in Werner (2001). The results are in good agreement with escape probabilities calculated from the exponential *Ansatz* (Amar et al. 2005) with the effective attenuation length λ set to 10 Å, and this value is henceforth adopted here.

3.2. Calculating Cluster–Monomer Shifts in S2p Ionization Energies

Time-dependent distributions of shifts in S2p ionization energy (IE) between the cluster and the monomer, i.e., $\Delta IE = IE(cluster) - IE(monomer)$, were calculated based on cluster geometries obtained from the last 200 ps of the trajectories. For each molecule at each cluster geometry, a unique ΔIE value is calculated and weighted by the probability that the photoelectron escapes from the cluster without undergoing inelastic scattering. The theoretical ΔIE value for the given cluster size and temperature is obtained as a time-average distribution of ionization energies. Contrary to what is the case for the experimentally determined ΔIE values, the calculated ΔIE values are based on single cluster sizes. However, in a recent study of CO_2 clusters (Harnes et al. 2011), it was found that the mean ionization energy for a log-normal distribution of clusters corresponds closely to the mean ionization energy of a cluster of size equal to the mean of the cluster distribution, $N = \langle N \rangle$. A similar result was previously reported for argon clusters (Bergersen et al. 2006a).

The calculation of shifts is based on a polarizable force field with an accurate description of the electrostatic potential around both the neutral and ionized molecules. In general, the force-field-predicted ΔIE values are found to be in good agreement with *ab initio* methods. For instance, the distribution of force-field-derived ΔIE values for a pentamer is bracketed by the corresponding results obtained by means of Møller-Plesset perturbation theory of 2nd order (MP2) (Møller and Plesset 1934) using two different but closely related basis sets (cc-pVTZ and aug-cc-pVTZ) (Dunning 1989; Kendall et al. 1992; Woon and Dunning Jr. 1993), respectively. Moreover, for an $N = 46$ cluster, the present approach to compute cluster–monomer shifts in ionization energy is validated against a combined quantum mechanics/molecular mechanics (QM/MM) approach. The agreement between the two models is very good except for an almost constant deviation between the QM and the MM estimates due to contributions from the first coordination shell of the site of ionization. A second source of error comes from a slight underestimation of the density at the force-field level of theory (see the SI). To correct for these small yet highly systematic errors, our theoretical estimate of the mean cluster–monomer shift, ΔIE_{theory}, is formed by adding the mean contribution from the first coordination shell, computed as $1.08\Delta IE_{FF,shell1} - 0.043$ eV, to that from all subsequent shells, computed as $1.04\Delta IE_{FF,shell>1}$. Here, ΔIE_{FF} denotes the corresponding force-field (FF)-based values.

The computational cost for force-field calculations that include mutual induction of dipoles at each atomic site and also a distributed electrostatic multipole description is substantial and increases fast with increasing cluster size (Ren et al. 2011). In order to obtain ΔIE values for clusters that are significantly larger than those propagated in the molecular dynamics simulations, we apply a polarizable continuum model as described in Björneholm et al. (1996) in combination with an exponential attenuation model (Amar et al. 2005; Bergersen et al. 2006a). Within the attenuation-dependent continuum model, the clusters are modeled as spheres. Each sphere is further divided into shells with thickness equal to $2^{1/6} \times n^{-1/3}$, which, for spherical particles in a face-centered-cubic packing, corresponds to twice the atomic radius. Here, n is the number density of solid SO_2 at 143 K (Post et al. 1952). By computing the ionization energy for a site in the middle of each shell, a radial distribution of ionization energies is obtained. The distribution of ionization energies is thereafter weighted according to the volume of each shell and by the probability that the photoelectron escapes from the cluster without undergoing inelastic scattering.

It is well known that the continuum approximation overestimates the polarization contribution to ΔIE from the nearest solvation shell (Björneholm et al. 1996). However, since the overestimation is of local origin, the difference between ΔIE values obtained using the continuum approximation and the force-field model, respectively, converges fast with cluster size. Reliable mean ΔIE values for large clusters may therefore be obtained as

$$\Delta IE_{N > 561} = \Delta IE_{N > 561,C} + \left(\Delta IE_{N = 561,FF} - \Delta IE_{N = 561,C} \right), \quad [2]$$

where the subscript C and FF denotes the continuum approximation and the force-field model, respectively.

3.3. The Cluster Temperature

The cluster temperature is an input parameter to the molecular dynamics simulations and affects the ΔIE values mainly through the density. The temperature may be estimated from a model that assumes the clusters to cool primarily by evaporation until reaching their so-called evaporative temperature, T_e, which in Pauly (2000) is approximated as $T_e = 0.04 \frac{\Delta u}{k_B}$. In this expression, Δu is the change in internal energy caused by the evaporation and k_B is the Boltzmann constant. Approximating Δu by the enthalpy of vaporization at the boiling point, $\Delta H_{vap} = 25.72$ kJ/mol (Yaws 1999), one obtains $T_e = 124$ K. Moreover, by plotting the experimental terminal cluster temperature (T_c) for a handfull of atomic and molecular clusters as given in Haberland (1994-1995b) vs. their respective boiling points (or sublimation temperatures), we obtain $T_c \approx 0.48 T_b$, where T_b is the boiling point or sublimation temperature at standard conditions, respectively. From $T_b = 263.16$ K (Yaws 1999) for SO_2, this empirical relationship suggests that T_c is about 126 K. Taking into account the relatively large uncertainty of T_c values in Haberland (1994-1995b), we estimate the terminal temperature for SO_2 clusters in this work to 125 ± 25 K.

4. RESULTS

Clusters were formed by adiabatically expanding pure SO_2 gas at high pressure into vacuum. The resulting beam of clusters and uncondensed monomers was subsequently probed by S2p photoelectron spectroscopy; see Figure 2 for a representative spectrum. The monomer contribution to the S2p spectrum appears as a spin-orbit-split doublet of sharp peaks near 174.8 eV and 176.0 eV in ionization energy. The cluster contribution to the spectrum consists of two broad peaks shifted to lower ionization energies compared to the monomer peaks. These form a spin-orbit doublet as described for the monomer, and each of these components reflects the combined signal from both surface and bulk parts of the clusters.

The most important observable from the photoelectron spectrum is the mean ionization energy of either of the cluster peaks. It is convenient to use the monomer line for internal reference, and hence we will focus on the mean cluster–monomer shift in $S2p_{3/2}$ ionization energy (ΔIE). The second important observable in the spectrum is the width of the $S2p_{3/2}$ cluster peak. However, since we describe this peak as a convolution between a monomer lineshape and a cluster-specific Gaussian broadening function, we will consistently use the full width at
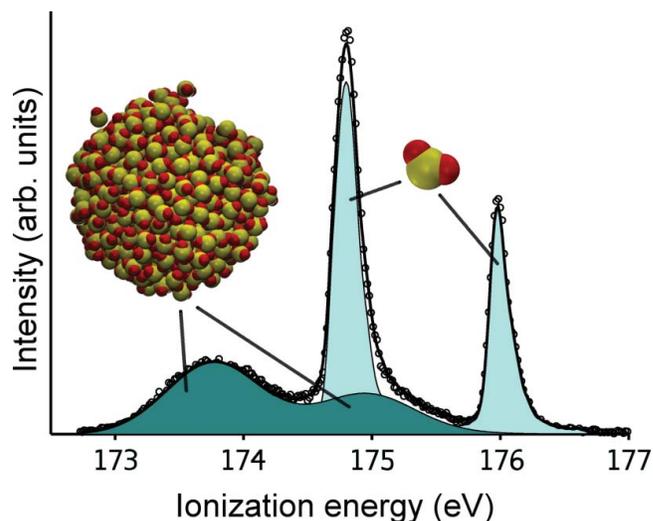

FIG. 2. S2p photoelectron spectrum (circles) of a beam of clusters and free monomers of SO_2 produced with a stagnation pressure of 1.97 bar and nozzle temperature of 301 K. The spectrum is decomposed into contributions from clusters (dark colored area) and free monomers (light color) by means of least-squares fitting as detailed in the text. Energy calibration is achieved by assigning the vertical $2p_{1/2}$ ionization energy of the monomer to 175.99(3) eV (Coville and Thomas 1995).

half maximum of the Gaussian distribution (fwhm$_G$) to characterize the width of the cluster peak.

Figure 3 shows the experimental spectra, recorded in 2009 and 2010 under 39 different expansion conditions and arranged vertically according to the corresponding value of the condensation parameter Γ^* (Figure 1). According to the principle of corresponding jets, expansions that are characterized by the same Γ^* value are similar with respect to cluster formation and end up with the same terminal mean cluster size, $\langle N \rangle$ (Hagena 1987). A word of caution is in place, as the gas-specific constant q appearing in the definition of Γ^* is not known for SO_2 and is here somewhat arbitrarily chosen equal to that of CO_2. Any realistic change in q would stretch

or compress the Γ^* axis slightly, but not affect any of qualitative conclusions to be drawn.

The maximum of the $2p_{3/2}$ cluster peak moves toward lower ionization energies with increasing Γ^* value, as indicated by the shaded area in Figure 3. This means that the cluster energy shift (ΔIE) increases in magnitude with increasing Γ^* value. The mean cluster size is generally expected to increase with Γ^*, thus implying that Figure 3, read from bottom to top, shows spectra in the order of increasing cluster size. The first spectrum at the bottom of Figure 3 is recorded at conditions corresponding to $\Gamma^* = 940$, showing that the onset of condensation takes place at conditions $\Gamma^* < 940$. In order to detect possible time-dependent variations in the experimental conditions, the 34 spectra from 2010 were recorded at alternating high and low Γ^* values. No time-dependent variations were observed, and the dataset is therefore believed to be of good quality with respect to both reproducibility and stability of experimental conditions.

To bring out more detailed information from the spectra, ΔIE and fwhm$_G$ are plotted toward Γ^* in the lower and upper parts of Figure 4, respectively. For $\Gamma^* \leq 5000$, ΔIE is seen to
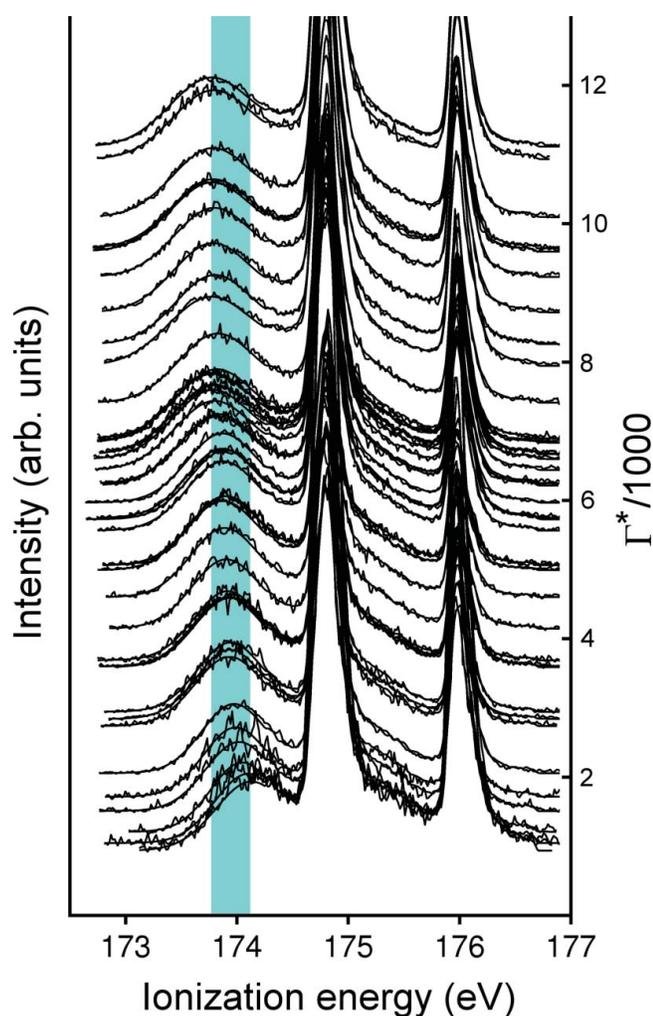

FIG. 3. Experimental and fitted S2p photoelectron spectra of cluster beams recorded at different conditions and arranged vertically according to increasing Γ^* value such that the high-energy tail of each spectrum indicates the corresponding Γ^* value. For details about the fitting, see caption of Figure 2. The shaded area marks the interval spanned by the maximum of the $2p_{3/2}$ cluster peak in the spectra corresponding to the lowest and highest Γ^* values, respectively.
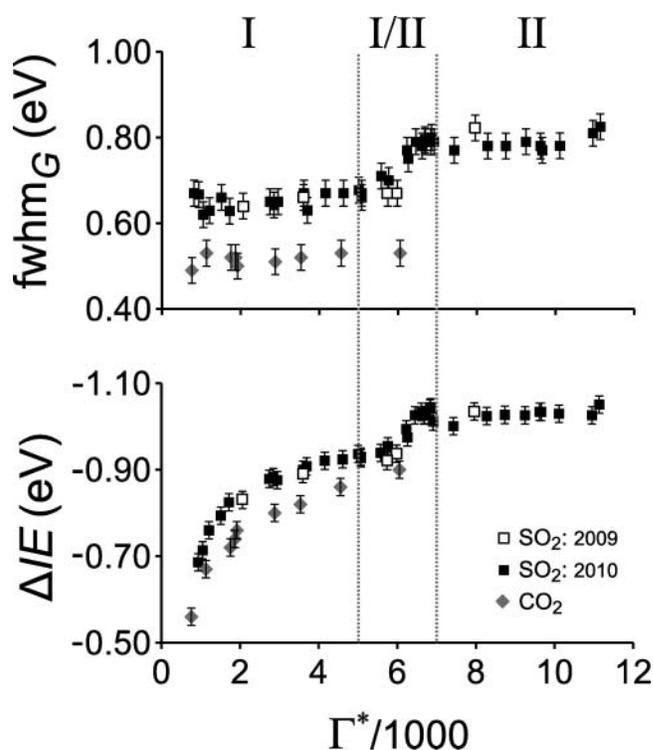

FIG. 4. The experimentally determined cluster–monomer shift in S2p ionization energies (open [2009] and filled [2010] squares), ΔIE (lower panel), and the width parameter fwhm$_G$ of the cluster peak (upper panel) plotted against the Γ^* condensation parameter; see Equation (S1) in the SI. The vertical dotted lines indicate the transition zone between two regimes I and II. Based on the fitting procedure, the uncertainties of ΔIE and fwhm$_G$ were determined as indicated at each data point by vertical bars. The corresponding C1s ΔIE and fwhm$_G$ values for CO_2 clusters are included for comparison (filled diamonds).

increase smoothly in magnitude, first quite steeply at low Γ^* values and then reaching a plateau at about -0.9 eV. For high $\Gamma^* \geq 7000$, on the other hand, ΔIE is constant at -1.03 eV within the experimental uncertainty. The development of ΔIE might be contrasted to that of fwhm$_G$, which appears almost constant in each of two highlighted intervals, but at different constant values of about 0.65 ($\Gamma^* \leq 5000$) and 0.79 eV ($\Gamma^* \geq 7000$), respectively. On the basis of these differences, it seems useful to introduce the notation of regions I and II as indicated in Figure 4. Regions I and II are separated by a transition zone in which both ΔIE and fwhm$_G$ change rapidly.

Interestingly, in region I, the evolution of ΔIE as a function of Γ^* shows large similarities to our recent findings (Harnes et al. 2011) for CO_2 clusters where the C1s cluster–monomer shift in ionization energy could be nicely fitted as a power function of Γ^*, suggesting that a similar approach may prove fruitful also for SO_2. We choose the functional form $\Delta IE = a\left(\frac{\Gamma^*}{1000}\right)^{-b} + c$, where a and b are left as fitting constants. Anticipating that $b > 0$, c is the high-Γ^* limiting value of the chemical shift assuming there are no phase or structural transitions as Γ^* increases. From MD simulations undertaken at 125 K and continuum-model calculations detailed toward the end of the *Results* section, we obtain a value of -1.11 eV for the theoretical ΔIE value for infinitely large clusters as shown in Equation (5) and Figure 8, and hence we fix $c = -1.11$ eV. The two remaining parameters a and b are determined by fitting to the experimental data in region I (Figure 5). The parameters show significant covariance and the error bar of the exponent (b) expresses the uncertainty associated with the final model where a was kept fixed.
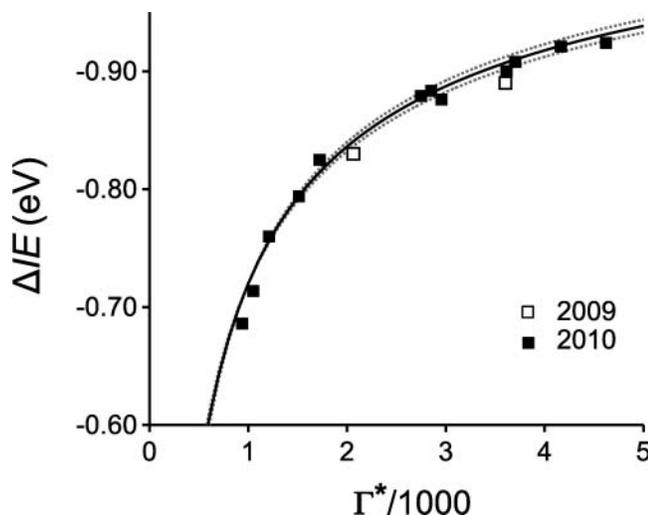
This error bar is estimated by refitting the model to 1000 sets of synthetic data prepared by adding noise to the original data points consistent with their respective uncertainties. The resulting fit is given in Equation (3).

$$\Delta IE = -1.11 \text{ eV} + 0.39 \text{ eV} \left(\frac{\Gamma^*}{1000}\right)^{-0.51(\pm 0.02)},$$

$$\text{where } \Gamma^* \in \{900, 5000\}. \qquad [3]$$

As confirmed in Figure 5, Equation (3) fits the experimental data well.

In the following, a relationship between ΔIE and cluster size is established by means of theory, and subsequently combined with Equation (3) to estimate cluster size from experimental conditions in region I. For region II, the theory-based ΔIE-$\langle N \rangle$ relationship will be used to show that the observed ΔIE value does in fact correspond to very large clusters. The sizeable jump in width of the cluster $S2p_{3/2}$ peak from region I to region II will be discussed in terms of possible structural changes.

4.1. ΔIE and fwhm$_G$ vs. Cluster Size

Figure 6 shows computed mean cluster–monomer shifts in ionization energy (ΔIE, bottom panel) as well as the full-width-at-half-maximum (fwhm$_G$, top panel) of Gaussian fits to theoretical models of S2p spectra as a function of cluster size. The theoretical spectra were prepared by convoluting the experimental monomer lineshape with computed distributions of S2p ionization energies taking into account signal attenuation in term of an effective attenuation length of $\lambda = 10$Å. The cluster geometries were generated by molecular dynamics simulations for five different cluster sizes (N = 13, 55, 147, 309, and 561), by propagation at three different temperatures: 100, 125, and 150 K. The aim of the simulations is to produce a distribution of realistic geometries that resemble the experimentally produced clusters of the selected size. Details of how the theoretical shift data were computed are given in the computational section.

The experimental S2p spectrum of a cluster beam reflects the distribution of ionization energies for each cluster size and is further broadened by intermolecular Franck-Condon effects and by the variation in mean shifts among the cluster sizes present in the beam. Our theoretical model spectrum, on the other hand, is based on the distribution of ionization energies within a single cluster, and a direct comparison of linewidths between theoretical and experimental spectra is not straightforward. However, in several recent studies (Bergersen et al. 2006a; Abu-samha et al. 2007; Harnes et al. 2011) on Ar and molecular clusters, it was demonstrated that except perhaps for the smallest clusters, broadening of the cluster peak is strongly dominated by the width of the distribution of vertical ionization energies for a single

FIG. 5. The cluster–monomer shift in S2p ionization energy, ΔIE, plotted against the condensation parameter, Γ^*. The squares show the experimental data points; open (2009) and black (2010). The black solid line represents Equation (3) while the dashed lines indicate the uncertainty associated with the exponential factor in Equation (3).
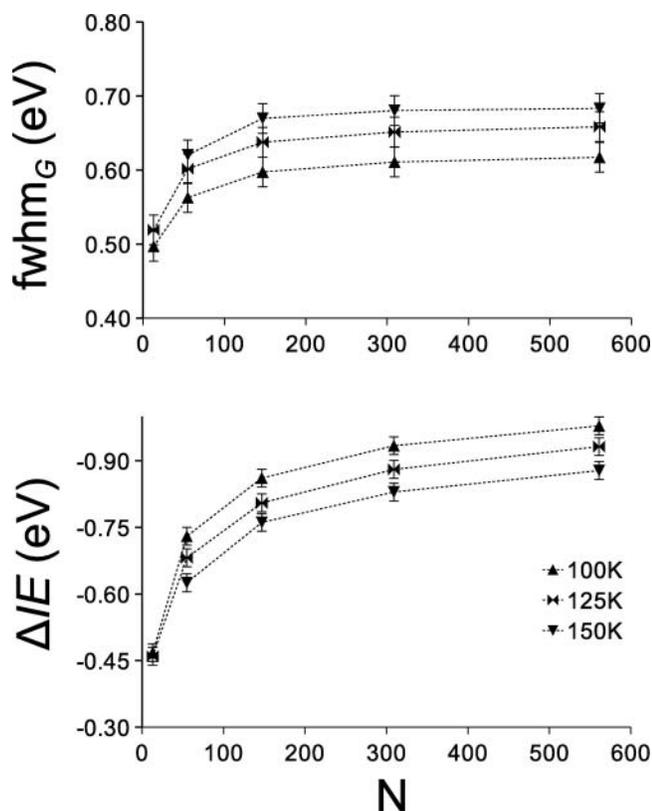
FIG. 6. Calculated mean value (ΔIE, bottom) and width (fwhm$_G$, top) of theoretical models of S2p photoelectron spectra, plotted against the number of molecules, N, in the cluster. The clusters were propagated at three different temperatures (100, 125, and 150 K). At each temperature, the uncertainties in calculated ΔIE and fwhm$_G$ values are estimated to 0.02 eV. The effective attenuation length λ is taken to be 10 Å.

(representative) cluster. Moreover, it was demonstrated that a cluster of size N equal to the mean of the cluster-size distribution, i.e., $N = \langle N \rangle$, is representative both in terms of reproducing the mean ionization energy of the cluster beam and the cluster-specific broadening of the cluster peak, fwhm$_G$. This may be surprising knowing that cluster size distributions are typically quite broad (Soler et al. 1982; Bobbert et al. 2002) and intuitively should contribute to the fwhm$_G$ parameter. However, convergence of the ionization energy with increasing cluster size suppresses the impact of the large-N tail of the size distribution on the spectral width and allows for our computed fwhm$_G$ values for large single-size clusters to be directly compared to the experimental fwhm$_G$ values.

From Figure 6, one can see that the mean shift value ΔIE decreases in magnitude with higher temperature, consistent with lower density. The width of the cluster peak increases with T, though, due to larger diversity in cluster structures. When comparing pairs of ΔIE and fwhm$_G$ of the computed distributions of ionization energies with the experimentally determined values, the agreement is best for data from simulations at 125 K. With this choice, Figure 7 demonstrates that the computed (shift, width) data points for the largest clusters
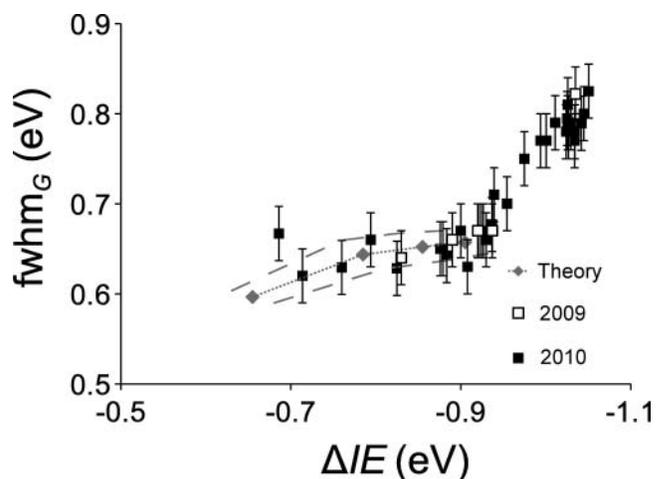

FIG. 7. Comparison of computed and experimentally determined fwhm$_G$ vs. ΔIE values. Computed values are shown for clusters of size $N = 55$, 147, 309, and 561, in geometries obtained from molecular dynamics simulations. The upper and lower dashed lines trace values obtained at 150 and 125 K, respectively, with diamonds marking the values obtained as the average of the 125 K and the 150 K data. Estimated error bars have been added to the experimental data points.

simulated ($N = 147$, 309, and 561) agree well with the experimentally determined data in region I; cf also the caption to Figure 4. An immediate conclusion based on the cluster–monomer shift is that in all experiments we produce clusters having a terminal mean size that is larger than or equal to about 50–60 molecules.

MD simulations have been carried out only for clusters up to size $N = 561$, corresponding to $\Delta IE \geq -0.93$ eV at $T = 125$ K and $\Delta IE \geq -0.88$ eV at $T = 150$ K. Many of the experimental data points are found outside the range spanned by the force-field-based calculations and in order to prepare theoretical shift data that apply to very large clusters, we make use of the continuum model as outlined in the computational section. The short-range correction in Equation (2) is fixed to 0.41 eV by comparison to the force-field-based shift for $N = 561$ as averaged over $T = 125$ K and 150 K. The corresponding values for the 125 and 150 K simulations are 0.38 eV and 0.44 eV, respectively.

$$\Delta IE_N = \Delta IE_{N,C} + 0.41 \text{ eV}, \quad N > 560 \qquad [4]$$

Figure 8 shows the ΔIE values computed using Equation (4). Following Jortner (1992) the computed ΔIE values are fitted to a linear function in $N^{-1/3}$, to give

$$\Delta IE_N = 1.68 N^{-1/3} \text{ eV} - 1.11 \text{ eV}. \qquad [5]$$

Equation (5) and Figure 8 show that our theoretical estimate of ΔIE converges toward -1.11 eV for the average of the 125 K and the 150 K data, and that ΔIE is most sensitive to
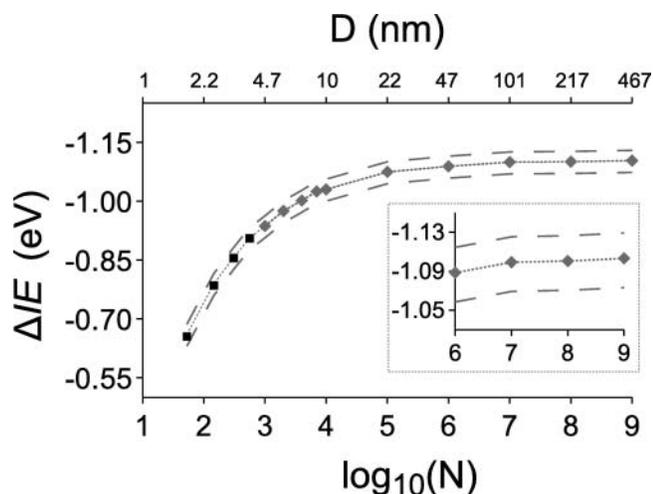
FIG. 8. Cluster–monomer shift in S2p ionization energy (ΔIE) is plotted vs. the number of molecules in the cluster (N, lower horizontal axis) and cluster diameter (D, upper horizontal axis) in the spherical-cluster approximation. The diameter is computed assuming a cluster density (1.92 g/cm^3) equal to that of crystalline SO_2 at 143 K (Post et al. 1952). ΔIE is calculated from Equation (4) as mean of the corresponding models parametrized toward theoretical shift data obtained from cluster structures obtained in MD simulations at 125 K and the 150 K, respectively. The upper and lower dashed lines trace values obtained using Equation (4) with the constant 0.41 eV replaced by 0.44 eV and 0.38 eV for the 150 K and 125 K data, respectively.

changes in size for clusters with diameter smaller than 10 nm, corresponding to clusters in the ultrafine particle range (Finlayson-Pitts and Pitts, Jr. 2000). The corresponding values for the 125 K and 150 K data are -1.13 eV and -1.08 eV, respectively. Combining Equations (3) and (5) with N replaced by $\langle N \rangle$ gives (Bergersen et al. 2006a; Harnes et al. 2011)

$$\langle N \rangle = 80 \left(\frac{\Gamma^*}{1000} \right)^{1.51(\pm 0.06)}, \text{ where } \Gamma^* \in \{900, 5000\}. \quad [6]$$

The error bar in Equation (6) is based solely on the uncertainty in the exponent in Equation (3). Equation (6) shows that $\langle N \rangle$ grows with Γ^* raised to the power of about 1.5. This exponential factor can be compared to suggested exponential factors for Ar (1.997) (Krauss et al. 1991), for H_2O (1.886) (Bobbert et al. 2002), for CO_2 (2.23) (Ramos et al. 2005; Harnes et al. 2011), and for NH_3 (1.348) (Bobbert et al. 2002).

Figure 4 shows that the experimentally determined ΔIE value stabilizes to -1.03 ± 0.02 eV in region II. The agreement between this value and the asymptotic value of the theoretical estimate in Equation (5) is good if we take the uncertainty in temperature and the uncertainty in the theoretical estimate into account. While Figure 8 shows that the theoretically ΔIE values have an asymptotic value of -1.13 eV for the 125 K data, the asymptotic value for the 150 K data is -1.08 eV. This suggests that the temperature may be somewhat higher for the clusters in region II compared to the clusters in region I.

However, based on the evolution of ΔIE toward Γ^* as shown in Figure 4, it seems that the experimental value of ΔIE has in fact converged to the large-cluster limit of the cluster–monomer shift in S2p ionization energy. Recently, Aksela et al. (2010) and Holappa et al. (2011) presented experimentally measured core-level solid–atom shift in ionization energy for Sb, Bi, K, and Rb. Due to problems with charging, the solid–monomer shift in ionization energy has not previously been obtained for insulators. To the best of our knowledge, this is the first time that such a quantity is probed experimentally.

5. DISCUSSION

Figure 4 shows that the magnitude of the cluster–monomer shift in S2p ionization energy and also the linewidth parameter of the cluster peak, fwhm$_G$, assume essentially constant values at stagnation conditions that in the course of this work are referred to as region II. Moreover, both of these quantities attain values that are significantly larger (in magnitude) than those observed in region I. It is to be noted that the reproducibility of the observations is very good, and hence these observations warrant an explanation. The question arises, what information do these observations convey about the evolution of SO_2 clusters with size? We start out by discussing implications from the observed evolution in ionization energy.

A preliminary assumption of no structural changes (apart from size) between clusters in regions I and II opens for applying the shift–size relationship obtained for region I also to the transition zone. In doing so, one finds from Figure 8 that the jump in ΔIE observed in the transition zone would correspond to a jump in cluster size from about $N = 600$ to $N \geq 9 \times 10^3$. This large increase in cluster size takes place within a rather narrow window of experimental conditions, i.e., for a stagnation pressure P_0 between 1.1 and 1.5 bar, which, according to Equation (6), would be expected to double the cluster size rather than to increase it ten-fold. At least one of the assumptions underpinning either the scaling law or the definition of the condensation parameters seems to be violated, implying that crossing the transition zone involves either a major change in cluster structure or access to a much more efficient mechanism for cluster growth than assumed in the Γ^* formalism, or both of these.

At this point it is useful to bring into discussion the complementary observation of the increase in cluster linewidth, fwhm$_G$, from region I to region II. The evolution of this quantity, with size as observed experimentally for both regions I and II in Figure 4 (top) and also computationally in Figure 6, suggests that fwhm$_G$ converges rather fast with size and significantly faster than does ΔIE. Hence, it appears that the significant jump in fwhm$_G$ cannot be explained solely by a jump in mean cluster size from region I to region II. On the other hand, from MD simulations of medium-sized clusters as reported in

Figure 6, the linewidth (fwhm$_G$) increases with increasing simulation temperature. Assuming this to apply also to large clusters, the increase in fwhm$_G$ from region I to region II may be rationalized as an increase in cluster temperature with size. This is, however, contradicted by the observed increase in the magnitude of ΔIE, as heating would in general lead to less negative ΔIE values (Figure 6, lower panel) through lower extra-molecular polarization with decreasing density. Moreover, it was shown for Ar clusters (Farges et al. 1981) that the terminal cluster temperature shows only a weak size dependency.

An alternative hypothesis for the observed increase in linewidth (fwhm$_G$) between clusters in regions I and II is a significant change in the contribution from extra-molecular electrostatic interactions to core ionization energies. This seems to require some kind of structural change, the most likely candidate being that of a phase transition, to which we turn next.

Bartell et al. (1989) report on the phase state of more than 50 different single-component clusters that were generated in supersonic beams, based on electron-diffraction measurements. The clusters had a diameter of about 10 nm, which, according to Figure 8, corresponds to clusters in the beginning of the transition zone between regions I and II. The phase state was found to correlate with an empirical index, $R_C = (T_b - T_m)/T_b + 0.007(\Delta S_m/R)^2$, where T_b and T_m are the boiling and melting temperatures at standard conditions, respectively, and ΔS_m is the entropy of melting. For compounds with $R_C < 0.32$, the clusters were found to be solid, while liquid clusters were produced if $R_C > 0.32$. For compounds with R_C close to 0.32, both the solid and the liquid phases could be produced. While the extensive list of compounds in Bartell et al. (1989) does not include SO_2, an R_C-value of 0.38 (Yaws 1999) suggests that SO_2 clusters in region I should be in the liquid phase. This result is also in line with our MD simulations at 125 K and 150 K, whereas at 100 K the cluster structures became rather glassy, i.e., amorphous but with little mobility.

It is well established that the melting temperature of nanoparticles depends on the cluster size, and except for a few anomalies, T_m is found to increase with size (Nimtz et al. 1988; Rytkönen et al. 1997; Mei and Lu 2007). Interestingly, the melting temperature changes by far the most at the smallest sizes, suggesting that it may be significantly larger at the end of region I compared to the beginning. Hence, while the cluster temperature probably increases slightly with size (Farges et al. 1981), the melting point changes much more, and at some size, the cluster temperature drops below the melting point. This implies a transition to solid clusters, with a slowly increasing degree of crystallinity with size. This view gets some support from vibrational-spectroscopy studies of pure SO_2 clusters. Signorell and Jetzki (2008) produced large SO_2 clusters (10^6 molecules) in a collisional cooling cell with helium as buffer gas and concluded that the clusters were partially amorphous in the temperature

range 20–80 K. Fleyfel et al. (1990) produced very large SO_2 clusters in an N_2 atmosphere and at higher temperatures of 80–130 K, with the conclusion that the clusters had crystalline structure.

In order to see the impact of structural order on the S2p spectrum, we constructed a constrained model of a cluster of size $N = 1181$ displaying a crystalline core. Starting from a spherical cut of crystalline SO_2 at 143 K (Post et al. 1952), a central core made up from the 253 molecules within a 15 Å radius from the center of mass was kept frozen in the crystalline structure while the remaining 79% of the cluster molecules were propagated under canonical-ensemble conditions at 125 K and with 1 fs timestep. The cluster surface soon undergoes surface relaxation (melting) and is propagated for 260 ps until reaching a stable value for the intermolecular interaction energy. The crystalline SO_2 core contains chains of zig-zagging molecules with one component of the dipole moment adding constructively. Past the core, there is a region with the molecular dipoles tending to be orthogonal to the core dipole, while the outer or molten part of the cluster is characterized by molecules with their dipoles oriented antiparallel to that of the core and benefiting from a favorable electrostatic interaction with the latter. This picture is evident from Figure 9, which shows the cartesian components of the dipole moment of spherical shells of thickness 1 Å from the cluster. The fully drawn line shows the dipole component that is parallel to the net dipole moment of the frozen core, while the other curves show the two components orthogonal to the first one.
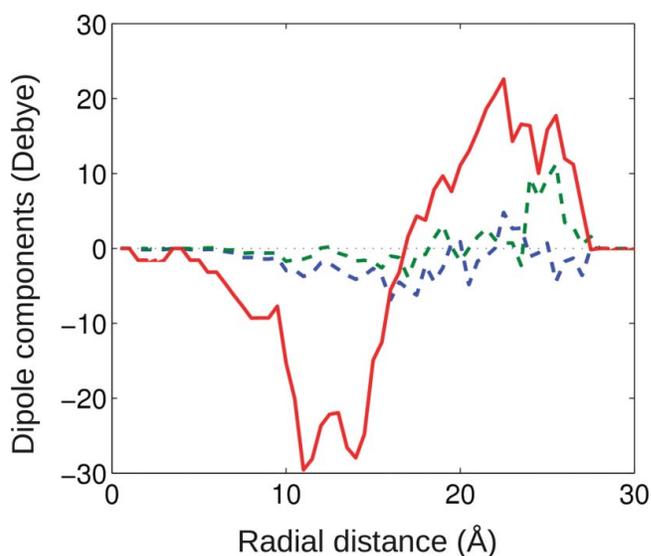

FIG. 9. Components of the mean electric dipole of molecules within a spherical shell at the indicated radial distance from the cluster center-of-mass, as obtained in a simulation of an $(SO_2)_{1181}$ cluster that is constrained to have the central 20% of the molecules in a crystalline arrangement. The fully drawn line corresponds to that direction of the net dipole of the crystalline core, whereas the two other lines refer to directions orthogonal to this. See text for more information.

When comparing computed values for the mean and root-mean-square deviation in the cluster–monomer shift in S2p ionization energy for our constrained cluster to those obtained for a fully relaxed cluster of the same size, some interesting differences appear. First, the difference in mean shift is small between the two models, amounting to about 0.05 eV compared to a mean shift of -0.83 eV. Next, the difference in peak width (fwhm) between the two distributions of shifts, is large, at 0.96 compared to 0.63 eV, respectively, as computed from the root-mean-square deviation from the mean in each case. While these findings support the idea that the formation of a crystalline core may increase the peak width appreciably without affecting the peak position much, they also show that either a small crystalline core or a semi-ordered larger core would be sufficient to account for the change in peak width that we observe between regions I and II.

In Figure 10a, the distribution of ionization energies in the outermost 10 Å shell of the cluster is decomposed into contributions from molecular polarization (ΔP) and interaction between permanent electrostatic moments (ΔM), such that ($\Delta IE = \Delta M + \Delta P$) (Abu-samha et al. 2007). While the polarization part is clearly dominant in deciding the magnitude of the chemical shift values, the permanent molecular moments are responsible for the rather large spread in ΔIE, corresponding to the width of the spectrum. Figure 10b demonstrates that ΔM is clearly correlated to the net dipolar potential from the frozen core, $e\Phi_\mu^{core}$, at the site of ionization. Also noteworthy is the fact that ΔM is largely centered about zero, showing how the frozen, dipolar cluster core acts to increase the width of the S2p XPS signal without affecting the mean ionization energy much.

According to Figure 4, both cluster–monomer shift and the width of the cluster peak evolve rapidly in the transition zone between regions I and II. While a structural transition from liquid or amorphous clusters to clusters with a partly frozen core may explain the increase in width, this does not seem to affect the mean ionization energy much. However, the evolution of a crystalline core, wrapped in a liquid surface layer with molecular dipoles that are partially oriented in the field from the former, does provide a mechanism for increasing cluster stability through stronger molecule–host cluster interaction with increasing size (Nanda et al. 2002), leading to lower saturation pressure, higher saturation ratio, and thereby larger clusters.

Alternatively, while the smaller clusters grow by monomer addition as assumed in the Γ^* formalism, in the absence of an inert carrier gas and with increasing stagnation pressure and cluster size, coalescence of clusters may possibly become a more efficient growth mechanism and give a strong increase in mean cluster size and a corresponding jump in cluster–monomer shift over a narrow interval of Γ^*. In addition to coagulation, the present system and observations may be of interest in the study of nonisothermal effects on particle growth, as these may be expected to be important in the absence of carrier gas (Pathak et al. 2013).

For CO_2 (Soler et al. 1982), N_2O (Echt et al. 1983), H_2O, and NH_3 (Bobbert et al. 2002), the transition between the two growth mechanisms was investigated and determined by means of mass spectrometry. In these studies, the working hypothesis was that the shape of the cluster size distribution would give information about the governing growth mechanism. More specifically, a cluster size distribution that is exponentially decaying with size was regarded to indicate cluster growth through monomer addition, while a log-normal would be consistent with growth through cluster coagulation. This hypothesis is contested (Söderlund et al. 1998; Feiden et al. 2008) and, moreover, other authors (Vostrikov and Dubov 2004) have underscored the importance of taking into account the size-dependency in the cluster stability with respect to evaporation of molecules.
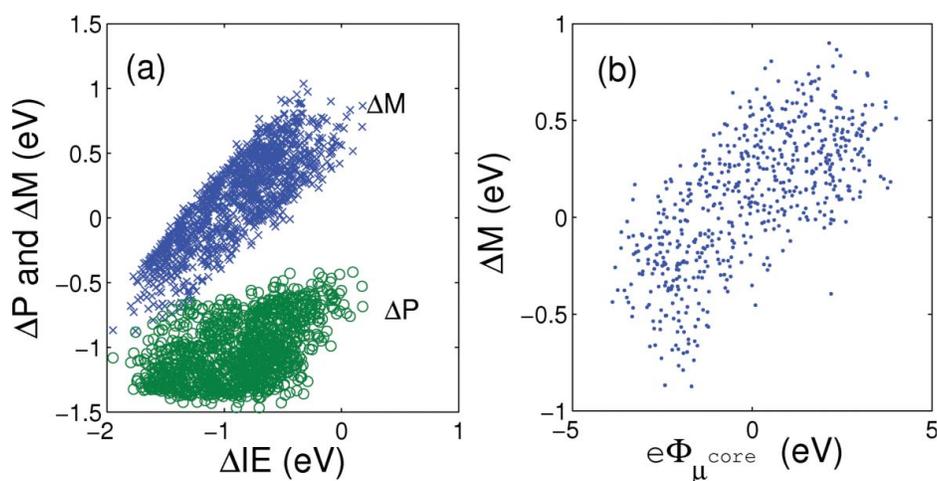

FIG. 10. Analysis of S2p ionization energies (relative to that of the free molecule) for the cluster model described in Figure 9 and in the text. (a) Decomposition of S2p shifts (ΔIE) into contributions from molecular polarization (ΔP) and permanent electrostatic moments (ΔM), and (b) ΔM vs. the net dipolar potential at the site of ionization, $e\Phi_\mu^{core}$, defined by the innermost 20% of molecules frozen to a crystalline core.

While the expression for the condensation parameter Γ^* is derived based on cluster growth through monomer addition, Bobbert et al. (2002) used the same formalism also for experimental conditions claimed to be consistent with cluster coalescence. For H_2O and NH_3, $\langle N \rangle$ seems to increase linearly with the logarithm of Γ^* for all cluster sizes investigated. Naively, one would expect a large increase in $\langle N \rangle$ when exceeding the Γ^* value that corresponds to the transition between the two growth regimes (Smirnov and Strizhev 1994) and hence the smooth evolution of $\langle N \rangle$ with Γ^* is surprising.

Recently, we used carbon 1s photoelectron spectroscopy to follow the size-evolution of CO_2 clusters as a function of expansion conditions (Harnes et al. 2011). $\langle N \rangle$ was found to grow smoothly with Γ^* for $\langle N \rangle$ between 50 and about 6000. In contrast to what was reported in Soler et al. (1982), no transition between growth regimes could be identified. This smooth evolution of $\langle N \rangle$ with Γ^* is in line with the observations made for H_2O and NH_3 in Bobbert et al. (2002). While this might suggest that $\langle N \rangle$ is rather insensitive to the growth mechanism, a more probable explanation is that the transition between the two growth mechanisms takes place at larger Γ^* values than probed in Harnes et al. (2011).

6. CONCLUSIONS

The formation of SO_2 clusters by adiabatic expansion is studied by means of core-level X-ray photoelectron spectroscopy and theoretical modeling. By carefully monitoring the evolution of the spectral properties as a function of expansion conditions, a transition between two different clustering regimes is found, suggested to differ in phase composition and mean size. At low-to-medium clustering conditions, liquid clusters are formed with mean size increasing to about 600 molecules as the stagnation pressure increases. Over a rather narrow range of higher values of the stagnation parameter, the S2p spectral observables undergo rapid and monotonous evolution and then stabilize at values that are consistent with theoretical simulations for large clusters having a partly crystalline interior and a molten surface.

SUPPLEMENTAL MATERIAL

Supplemental data for this article can be accessed on the publisher's website.

REFERENCES

Abu-samha, M., Børve, K. J., Harnes, J., and Bergersen, H. (2007). What Can C1s Photoelectron Spectroscopy Tell About Structure and Bonding in Clusters of Methanol and Methyl Chloride? *J. Phys. Chem. A*, 111:8903–8909.

Aksela, S., Patanen, M., Urpelainen, S., and Aksela, H. (2010). Direct Experimental Determination of Atom-Molecule-Solid Binding Energy Shifts for Sb and Bi. *New J. Phys.*, 12:063003.

Amar, F. G., Smaby, J., and Preston, T. J. (2005). Simulating the Photoelectron Spectra of Rare-Gas Clusters. *J. Chem. Phys.*, 122:244717.

Bartell, L. S., Harsanyi, L., and Valente, E. J. (1989). Phases and Phase Changes of Molecular Clusters Generated in Supersonic Flow. *J. Phys. Chem.*, 93:6201–6205.

Bässler, M., Ausmees, A., Jurvansuu, M., Feifel, R., Forsell, J.-O., de Tarso Fonseca, P., Kivimäki, A., Sundin, S., Sorensen, S. L., Nyholm, R., Björneholm, O., Aksela, S., and Svensson, S. (2001). Beam Line I411 at MAX-II - Performance and First Results. *Nucl. Instr. Meth. Phys. Res. A*, 469:382–393.

Bässler, M., Forsell, J.-O., Björneholm, O., Feifel, R., Jurvansuu, M., Aksela, S., Sundin, S., Sorensen, S. L., Nyholm, R., Ausmees, A., and Svensson, S. (1999). Soft X-Ray Undulator Beam Line I411 at MAX-II for Gases, Liquids and Solid Samples. *J. Electron Spectrosc. Relat. Phenom.*, 101–103:953–957.

Bergersen, H., Abu-samha, M., Harnes, J., Björneholm, O., Svensson, S., Sæthre, L. J., and Børve, K. J. (2006a). Size of Neutral Argon Clusters From Core-Level Photoelectron Spectroscopy. *Phys. Chem. Chem. Phys.*, 8:1891–1898.

Bergersen, H., Abu-samha, M., Lindblad, A., Marinho, R. R. T., Céolin, D., Öhrwall, G., Sæthre, L. J., Tchaplyguine, M., Børve, K. J., Svensson, S., and Björneholm, O. (2006b). First Observation of Vibrations in Core-Level Photoelectron Spectra of Free Neutral Molecular Clusters. *Chem. Phys. Lett.*, 429:109–113.

Berndt, T., Böge, O., Stratmann, F., Heintzenberg, J., and Kulmala, M. (2005). Rapid Formation of Sulfuric Acid Particles at Near-Atmospheric Conditions. *Science*, 307:698–700.

Bhardwaj, A., and Michael, M. (1999). Monte Carlo Model for Electron Degradation in SO_2 Gas: Cross Sections, Yield Spectra, and Efficiencies. *J. Geophys. Res.*, 104:24713–24728.

Björneholm, O., Federmann, F., Fössing, F., Möller, T., and Stampfli, P. (1996). Core Level Binding Energy Shifts and Polarization Screening: A Combined Experimental and Theoretical Study of Argon Clusters. *J. Chem. Phys.*, 104:1846–1854.

Bobbert, C., Schütte, S., Steinbach, C., and Buck, U. (2002). Fragmentation and Reliable Size Distributions of Large Ammonia and Water Clusters. *Eur. Phys. J. D*, 19:183–192.

Coville, M., and Thomas, T. D. (1995). Sulfur 2p Ionization Energies of H_2S, OCS, SO_2, and CS_2. *J. Electron Spectrosc. Relat. Phenom.*, 71:21–23.

Dong, F., Heinbuch, S., Rocca, J. J., and Bernstein, E. R. (2006). Single Photon Ionization of van Der Waals Clusters With a Soft X-Ray Laser: $(SO_2)(n)$ and $(SO_2)(n)(H_2O)(m)$. *J. Chem. Phys.*, 125:154317.

Dunning, Jr., T. H. (1989). Gaussian-Basis Sets for Use in Correlated Molecular Calculations. 1. The Atoms Boron Through Neon and Hydrogen. *J. Chem. Phys.*, 90:1007–1023.

Echt, O., Knapp, M., Sattler, K., and Recknagel, E. (1983). Mass-Spectrometric Size Analysis of N_2O-Clusters. *Z. Phys. B*, 53:71–74.

Ezell, M. J., Chen, H., Arquero, K. D., and Finlayson-Pitts, B. J. (2014). Aerosol Fast Flow Reactor for Laboratory Studies of New Particle Formation. *J. Aerosol Sci.*, 78:30–40.

Farges, J., Feraudy, M. F. D., Raoult, B., and Torchet, G. (1981). Structure and Temperature of Rare-Gas Clusters in a Supersonic Expansion. *Surf. Sci.*, 106:95–100.

Feiden, P., Stehlé, J., and Leygnier, J. (2008). Growth of Gas Phase Nanoparticles With an Accretion Mechanism. *Eur. Phys. J. D*, 50:53–60.

Finlayson-Pitts, B. J. (2009). Reactions at Surfaces in the Atmosphere: Integration of Experiments and Theory as Necessary (But Not Necessarily Sufficient) for Predicting the Physical Chemistry of Aerosols. *Phys. Chem. Chem. Phys.*, 11:7760–7779.

Finlayson-Pitts, B. J., and Pitts, Jr., J. N. (2000). *Chemistry of the Upper and Lower Atmosphere*. Academic Press, London, pp. 354–355.

Fleyfel, F., Richardson, H. H., and Devlin, J. P. (1990). Comparative SO_2 Infrared-Spectra: Type-I and Type-II Clathrate Hydrate Films, Large Gas-Phase Clusters, and Anhydrous Crystalline Films. *J. Phys. Chem.*, 92:7032–7037.

Haberland, H., ed. (1994–1995a). *Clusters of Atoms and Molecules I & II, vol. 52 and 56 of Springer Series in Chemical Physics*. Springer, Berlin.

Haberland, H., ed. (1994–1995b). *Clusters of Atoms and Molecules I, volume 52 of Springer Series in Chemical Physics*. Springer, Berlin, p. 216.

Hagena, O. F. (1969). in *Rarefied Gas Dynamics, Vol. II*, L. Trilling and H. Y. Wachman, eds., Academic, New York, p. 1465.

Hagena, O. F. (1974a). Scaling Laws for Condensation in Nozzle Flows. *Phys. Fluids*, 17:894–896.

Hagena, O. F. (1974b). in *Molecular Beams and Low Density Gas Dynamics*, P. P. Wegener, ed., Marcel Dekker, New York, pp. 93–181.

Hagena, O. F. (1981). Nucleation and Growth of Clusters in Expanding Nozzle Flows. *Surf. Sci.*, 106:101–116.

Hagena, O. F. (1987). Condensation in Free Jets: Comparison of Rare Gases and Metals. *Z. Phys. D*, 4:291–299.

Hagena, O. F. (1992). Cluster Ion Sources. *Rev. Sci. Instrum.*, 63:2374–2379.

Hagena, O. F., and Obert, W. (1972). Cluster Formation in Expanding Supersonic Jets: Effect of Pressure, Temperature, Nozzle Size, and Test Gas. *J. Chem. Phys.*, 56:1793–1802.

Harnes, J., Winkler, M., Lindblad, A., Sæthre, L. J., and Børve, K. J. (2011). The Size of Free Neutral CO_2 Clusters From Carbon 1s Ionization Energies. *J. Phys. Chem. A*, 115:10408–10415.

Holappa, M., Aksela, S., Patanen, M., Urpelainen, S., and Aksela, H. (2011). Atom-Solid Binding Energy Shifts for K 2p and Rb 3d Sublevels. *J. Electron Spectrosc. Rel. Phenom.*, 184:371–374.

Johnston, R. L. (2002). *Atomic and Molecular Clusters*. Taylor & Francis, London.

Jortner, J. (1992). Cluster Size Effects. *Z. Phys. D*, 24:247–275.

Kendall, R. A., Dunning, Jr., T. H., and Harrison, R. J. (1992). Electron-Affinities of the 1st-Row Atoms Revisited: Systematic Basis-Sets and Wave-Functions. *J. Chem. Phys.*, 96:6796–6806.

Krauss, J., de Vries, J., Steger, H., Kaiser, E., Kamke, B., and Kamke, W. (1991). TPEPICO Studies Near Ionization Threshold of Argon and Krypton Clusters. *Z. Phys. D*, 20:29–32.

Kulmala, M., Pirjola, L., and Mäkelä, J. M. (2000). Stable Sulphate Clusters as a Source of New Atmospheric Particles. *Nature*, 404:66–69.

Laksmono, H., Tanimura, S., Allen, H. C., Wilemski, G., Zahniser, M. S., Shorter, J. H., Nelson, D. D., McManus, J. B., and Wyslouzil, B. E. (2011). Monomer, Clusters, Liquid: An Integrated Spectroscopic Study of Methanol Condensation. *Phys. Chem. Chem. Phys*, 13:5855–5871.

Mei, Q. S., and Lu, K. (2007). Melting and Superheating of Crystalline Solids: From Bulk to Nanocrystals. *Prog. Mater. Sci.*, 52:1175–1262.

Møller, C., and Plesset, M. S. (1934). Approximation Treatment for Many-Electron Systems. *Phys. Rev.*, 46:618–622.

Nanda, K. K., Kruis, F. E., and Fissan, H. (2002). Evaporation of Free PbS Nanoparticles: Evidence of the Kelvin Effect. *Phys. Rev. Lett.*, 89:256103.

Nimtz, G., Marquardt, P., Stauffer, D., and Weiss, W. (1988). Raoult's Law and the Melting Point Depression in Mesoscopic Systems. *Science*, 242:1671–1672.

Ota, S. T., and Richmond, G. L. (2011). Chilling Out: A Cool Aqueous Environment Promotes the Formation of Gas-Surface Complexes. *J. Am. Chem. Soc.*, 133:7497–7508.

Paci, P., Zvinevich, Y., Tanimura, S., Wyslouzil, B. E., Zahniser, M. S., Shorter, J. H., Nelson, D. D., and McManus, J. B. (2004). Spatially Resolved Gas Phase Composition Measurements in Supersonic Flows Using Tunable Diode Laser Absorption Spectroscopy. *J. Chem. Phys.*, 121:9964–9970.

Pathak, H., Mullick, K., Tanimura, S., and Wyslouzil, B. E. (2013). Nonisothermal Droplet Growth in the Free Molecular Regime. *Aerosol Sci. Technol.*, 47:1310–1324.

Pauly, H. (2000). *Atom, Molecule, and Cluster Beams I*. Springer, Berlin.

Ponder, J. W., and Richards, F. M. (1987). Tinker: Software Tools for Molecular Design, Version 4.2. *J. Comput. Chem.*, 8:1016–1024.

Ponder, J. W., Wu, C., Ren, P., Pande, V. S., Chodera, J. D., Schnieders, M. J., Haque, I., Mobley, D. L., Lambrecht, D. S., DiStasio, Jr., R. A., Head-Gordon, M., Clark, G. N. I., Johnson, M. E., and Head-Gordon, T. (2010). Current Status of the AMOEBA Polarizable Force Field. *J. Phys. Chem. B*, 114:2549–2564.

Post, B., Schwartz, R. S., and Fankuchen, I. (1952). The Crystal Structure of Sulfur Dioxide. *Acta Cryst.*, 5:372–374.

Ramos, A., Fernández, J. M., Tejeda, G., and Montero, S. (2005). Quantitative Study of Cluster Growth in Free-Jet Expansions of CO_2 by Rayleigh and Raman Scattering. *Phys. Rev. A*, 72:053204.

Ren, P., Wu, C., and Ponder, J. W. (2011). Polarizable Atomic Multipole-Based Molecular Mechanics for Organic Molecules. *J. Chem. Theory Comput.*, 7:3143–3161.

Rytkönen, A., Valkealahti, S., and Manninen, M. (1997). Melting and Evaporation of Argon Clusters. *J. Chem. Phys.*, 106:1888–1892.

Shvartsburg, A. A., and Jarrold, M. F. (2000). Solid Clusters Above the Bulk Melting Point. *Phys. Rev. Lett.*, 85:2530–2532.

Signorell, R., and Jetzki, M. (2008). Vibrational Exciton Coupling in Pure and Composite Sulfur Dioxide Aerosols. *Faraday Discuss.*, 137:51–64.

Smirnov, B. M., and Strizhev, A. J. (1994). Kinetics of Clustering Processes in Expanding Vapor. *Physica Scripta.*, 49:615–618.

Söderlund, J., Kiss, L. B., Niklasson, G. A., and Granqvist, C. G. (1998). Log-normal Size Distributions in Particle Growth Processes Without Coagulation. *Phys. Rev. Lett.*, 80:2386–2388.

Soler, J. M., Garcìa, N., Echt, O., Sattler, K., and Recknagel, E. (1982). Microcluster Growth: Transition From Successive Monomer Addition to Coagulation. *Phys. Rev. Lett.*, 49:1857–1860.

Tchaplyguine, M., Feifel, R., Marinho, R. R. T., Gisselbrecht, M., Sorensen, S. L., Naves de Brito, A., Mårtensson, N., Svensson, S., and Björneholm, O. (2003). Selective Probing of the Electronic Structure of Free Clusters Using Resonant Core-Level Spectroscopy. *Chem. Phys.*, 289:3–13.

Vostrikov, A. A., and Dubov, D. Y. (2004). Clustering in Molecular Gases Freely Expanding into Vacuum. *J. Exp. Theo. Phys.*, 98:197–206.

Werner, W. S. M. (2001). Electron Transport in Solids for Quantitative Surface Analysis. *Surf. Interface Anal.*, 31:141–176.

Woon, D. E., and Dunning, Jr., T. H. (1993). Gaussian Basis Sets for Use in Correlated Molecular Calculations. III. The Atoms Aluminum Through Argon. *J. Chem. Phys.*, 98:1358–1371.

Yaws, C. L. (1999). *Chemical Properties Handbook*. McGraw-Hill, New York.

Yoder, B. L., Litman, J. H., Forysinski, P. W., Corbett, J. L., and Signorell, R. (2011). Sizer for Neutral Weakly Bound Ultrafine Aerosol Particles Based on Sodium Doping and Mass Spectrometric Detection. *J. Phys. Chem. Lett.*, 2:2623–2628.